Kovove Mater. 57 2019 407–414
DOI: 10.4149/km_2019_6_407

High-temperature deformation properties of CuCr0.6 alloy

S. Rusz[1]*, I. Schindler[1], H. Navrátil[1], P. Kawulok[1], K. Rodak[2], R. Kawulok[1], P. Opěla[1], V. Ševčák[1]

[1] *VŠB – Technical University of Ostrava, Faculty of Materials Science and Technology, 17. listopadu 15, 708 00 Ostrava, Czech Republic*
[2] *Silesian University of Technology, Faculty of Materials Engineering and Metallurgy, Krasińskiego 8, 40 019 Katowice, Poland*

Received 11 April 2019, received in revised form 17 May 2019, accepted 28 June 2019

Abstract

The submitted paper aimed to investigate the hot deformation behavior of CuCr0.6 alloy. Nil strength temperature of 1349 K and nil ductility temperature of 1313 K have been experimentally determined. Formability is monotonously increased with the decrease of forming temperature in the temperature range from 923 K to approx. 1273 K. The flow stress curves were obtained in the forming temperature interval of 923–1223 K and at a strain rate of 0.1–10 s^{-1}. After their analysis, the hot deformation activation energy of 340 kJ mol^{-1} was calculated for peak stress and 393 kJ mol^{-1} for steady state. This proves that the value of the activation energy depends upon a strain size.

K e y w o r d s: copper alloy CuCr0.6, nil strength temperature, nil ductility temperature, flow stress curves, hot deformation activation energy

1. Introduction

Selection of the optimum properties of the material for electrical applications always involves balancing between the mechanical and electrical properties. Annealed high-purity copper exhibits high electrical conductivity but low strength. Strengthening procedures (via the introduction of foreign atoms into a solid solution and/or cold deformation) yield more or less in the electrical conductivity degradation. Precipitation-hardened Cu-Cr alloys exhibit a favorable combination of the strength and electrical properties. They can be used as materials for welding electrodes, seam welding wheels, shafts and bearings, electric motor and generator components, thermal conductors, railway contact wires, parts for electronic devices, etc. [1–3]. Many severe plastic deformation (SPD) methods are considered to ensure an ultrafine-grained microstructure of the Cu-Cr alloys with good strength and physical properties. Tensile strength and electrical conductivity were enhanced in Cu-Cr-Zr alloys after the equal-channel angular pressing (ECAP) and aging treatment [4]. Ultrafine-grained (UFG) commercial Cu alloy with 0.5 % Cr was fabricated by the aging treatment followed either by ECAP or by 80 % cold rolling. The final properties were comparable after rolling and/or 4 ECAP passes [5]. Wei et al. processed the Cu-0.5 %Cr alloy by 4 ECAP passes, followed by 90 % cold rolling. Better comprehensive properties, namely, ultimate tensile strength (UTS) 554 MPa and electrical conductivity 84 % of IACS (International Annealed Copper Standard), were obtained by additional aging at 450 ℃ for 1 h [6]. Dobatkin et al. studied the properties of UFG microstructures in Cu alloy for different chromium contents (0.75, 9.85, and 27 %); the samples were processed by high-pressure torsion (HPT) [1]. Nanostructuring of the Cu-Cr alloy by HPT led to a combination of the high ultimate tensile strength of 790 to 840 MPa, enhanced the electrical conductivity of 81 to 85 % of IACS and thermal stability up to 500 ℃ [7]. Compression with oscillatory torsion (COT) processing with different values of the total effective strain (up to 40) was introduced to CuCr0.6 material. The aging process supported the grain refinement to the size of 300 nm during COT processing. Simultaneously, the

*Corresponding author: e-mail address: stanislav.rusz2@vsb.cz

COT technique appears to be most effective in the strengthening of this alloy under precipitation hardening conditions [8]. Several experimental works confirmed the possibility of using repetitive corrugation and straightening (RCS) to increase the mechanical properties of CuCr0.6 alloy [9, 10]. Precipitation processes in CuCr0.7 alloy were studied by Rdzawski et al. The samples were subjected to treatment by supersaturation (950 °C for 1 h), cold rolling with 50 % reduction and aging. Electrical conductivity was significantly changing: 20.5 MS m^{-1} after quenching vs 49.4 MS m^{-1} after quenching, deformation and aging at 550 °C for 420 min [11]. Massive effect of rolling with the cyclic movement of rolls (RCMR) was demonstrated by Kinga et al. for the CuCr0.6 alloy properties. UTS rose from 214 MPa (initial state) to 393 MPa after SPD and to 539 MPa after the subsequent aging treatment at 500 °C for 2 h. Electrical conductivity increased to 83 % IACS [12].

Properties of copper alloys and the structure-forming processes associated with their bulk-forming are in interest to many researchers, but there is relatively little information about their hot deformation behavior. The testing conditions are mostly based on the specific experimental possibilities, especially for the tensile tests performed on devices such as INSTRON. Wider testing conditions are achieved by the compression tests performed on special equipment – see e.g. [13]. It is quite understandable why there is a lack of comprehensive data on the hot deformation behavior of copper alloys, especially in terms of their formability. The most widespread Gleeble hot deformation simulators can be only with difficulties used to carry out hot tensile tests on copper samples because they cannot hold the conventionally welded thermocouples in the course of their resistance heating. This can be solved by fastening the thermocouple wires into a small drilled hole, which, however, negatively affects elongation to fracture [14]. In the case of hot compression tests, the situation is much simpler and therefore this method is more popular for copper alloys.

2. Aim of work and material investigated

The aim of the experimental work was to complexly investigate the hot deformation behavior of CuCr0.6 precipitation-hardened copper alloy with 0.6 wt.% Cr and 0.1 wt.% P (C18200) to determine its hot formability and flow curves in the widest possible range of forming conditions. The results should help to optimize the real processes of hot bulk-forming of the examined material.

The material was prepared by melting and alloying in the open-air induction furnace. The resulting castings were approximately of dimensions Ø 20 mm × 300 mm. On a semi-continuous laboratory rolling mill, rods Ø 9.8 mm were rolled out, with a total of 6 passes using the flat oval and round grooves. The material temperatures ranged from 993 to 1173 K with two interoperative heatings applied. The rolled rods were uniformly heat treated in the electric resistance furnace with the mode of 973 K/15 min at temperature/air.

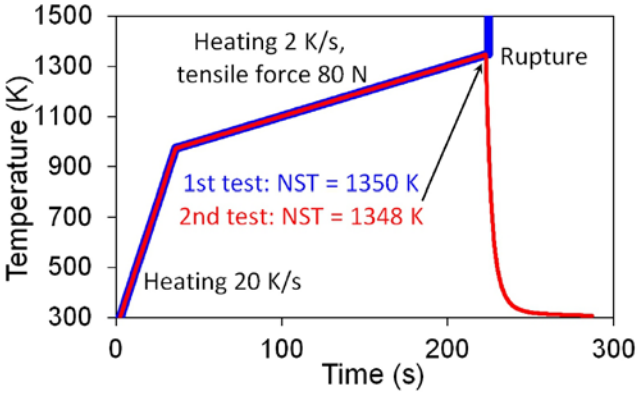

Fig. 1. The course of the tests in determining the NST value.

3. Experimental methods and discussion of results

Altogether four various test types were performed on the Hot Deformation Simulator Gleeble 3800 and its Model 39112 Scanning Non-Contact Optical Dilatometer System to evaluate the hot deformation behavior of the tested copper alloy.

3.1. Nil strength temperature

Nil strength temperature (NST) was determined by a special procedure. The anisothermal test is based on the gentle tensile stress of the samples Ø 6 mm × 81 mm by the small constant force of 80 N with the simultaneous linear increase of the temperature up to the moment of the fracture. As documented by Fig. 1, NST = 1349 K for the tested alloy. This high value of NST is in the surprising accordance with the assumed eutectic transformation temperature of 1350 K (compare with Fig. 2 [15]). The fracture surface in Fig. 3 shows the signs of partial melting of the sample.

3.2. Hot ductility

The influence of the deformation temperature on the formability of the examined alloy has been investigated based on the set of tensile tests to rupture at selected piston rate. The uniaxial tensile tests used the samples of Ø 6 mm × 116.5 mm which were re-

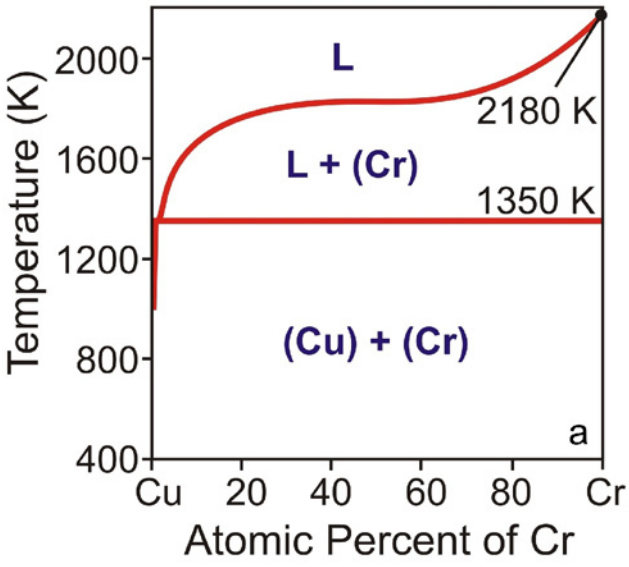

Fig. 2. Cu-Cr phase equilibrium diagram – according to [15].

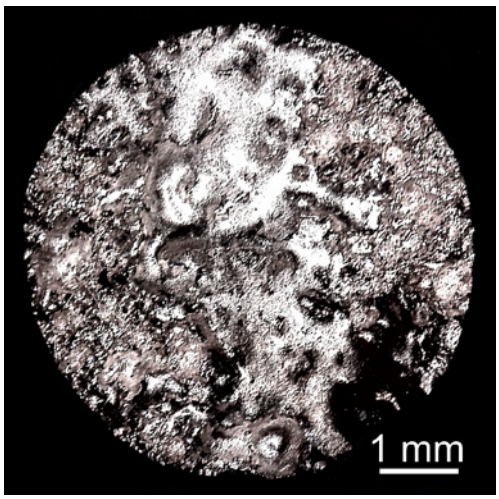

Fig. 3. Fracture surface morphology after the NST test.

sistively heated on the measured length $L_0 = 20$ mm at a rate of 10 K s^{-1} immediately to the deformation temperature ranging from 923 to 1323 K. Sample elongation to break was evaluated after a delay of 180 s at deformation temperature. The applied stroke rate of 100 mm s^{-1} yielded in a mean true strain rate of approx. 5 s^{-1}. From the computerized data, tensile strength (MPa) and relative elongation to break (%) related to the L_0 value were calculated. It should be kept in mind that the observed elongation values were influenced by the holes drilled into the samples to attach the thermocouple wires [14]. Thus, the elongation to break values cannot be understood as absolute but

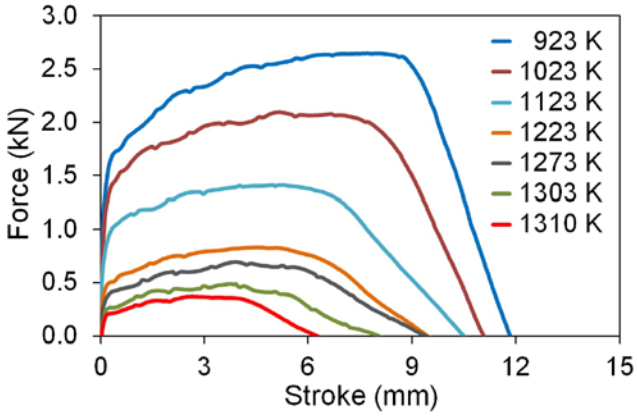

Fig. 4. Force-stroke dependence in the selected tensile tests.

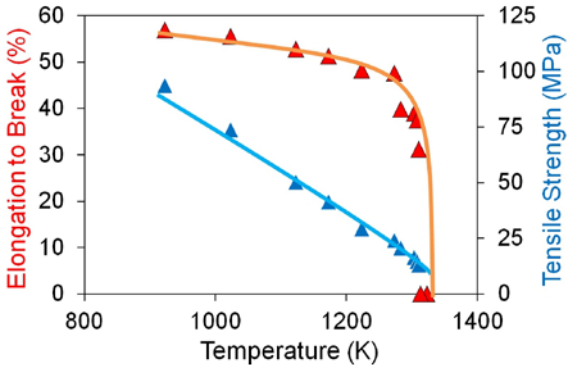

Fig. 5. Temperature dependence of ductility and tensile strength.

only as giving the possibility to determine the trends of the temperature dependence of ductility.

The course of the selected tensile tests is compared in Fig. 4. The results are in the entire temperature range more or less monotonous – flow stress and even formability are decreased with the increasing temperature. This, however, is atypical – the formability of metal materials is mostly declined by the decreasing temperature [16, 17].

This fact is in a well-arranged manner documented by the graph in Fig. 5. The strength almost linearly descends to the temperature of about 1310 K. The sharp drop of ductility due to overheating and burning of the material was observed above the temperature of approx. 1273 K. The nil ductility temperature NDT = 1313 K could be determined, which corresponds to the experimentally determined value of NST = 1349 K.

The temperature course of ductility has not been signalizing any significant phase transformation. Nevertheless, the change of the trend at the temperature of ca 1023 K has been revealed in the case of the dilatometric curve which was acquired during the resistance

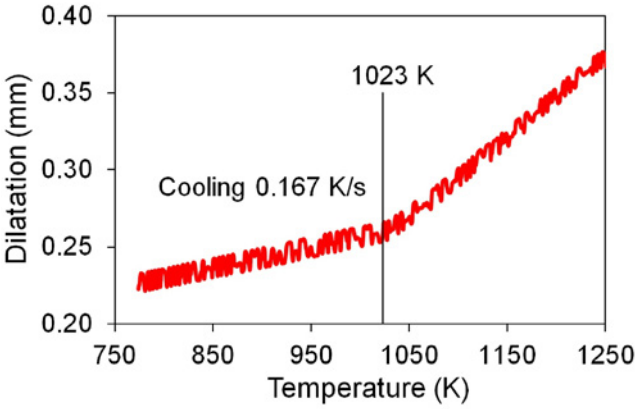

Fig. 6. Dilatometric curve recorded during cooling.

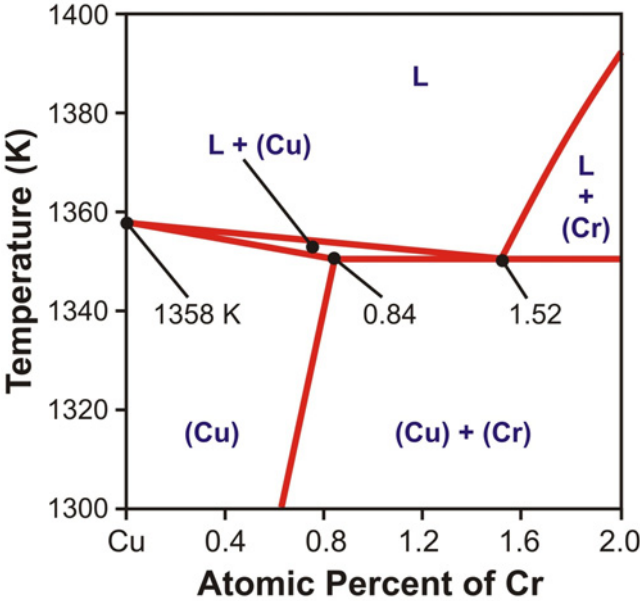

Fig. 7. Detail of the Cu-Cr phase equilibrium diagram near the (Cu)-phase liquidus line –according to [18].

heating (at max. temperature of 1273 K) and subsequent cooling of the sample Ø 6 mm × 86 mm at the rate of 1 K s^{-1} (see Fig. 6). The reason for this can be only explained by the precipitation of the chromium particles [12] (compare with the equilibrium phase diagram in Fig. 7 [18]). This transformation is probably too stable to significantly influence the formability.

The microstructure of samples heated to 1023, 1273, and 1313 K was fixed by water quenching and subjected to optical metallography – see Fig. 8. In all cases, the structure is composed of the fully recrystallized FCC grains of copper, in which the second phase is formed by the fine and uniformly distributed chromium particles whose dimensions are usually below 1 µm. The grain size markedly grows with the increasing temperature of heating. The presence of particles in the microstructure indicates a lack of chromium solubility in the matrix.

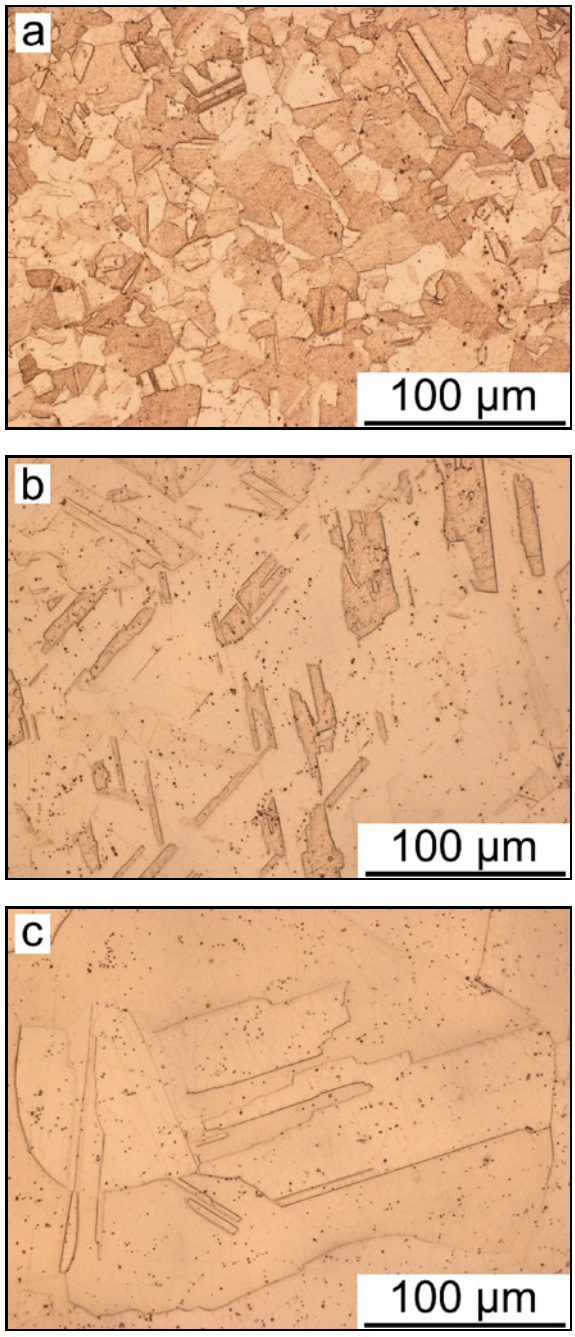

Fig. 8. Microstructure of the samples quenched from temperature: (a) 1023 K; (b) 1273 K; (c) 1313 K.

The CuCr0.6 (C18200) alloy generally shows a good capacity for being hot formed at the temperature range of 1089–1200 K and 700–769 K (see the datasheet accessible at [19]). The performed tensile tests have proved good formability in the wider temperature range, at least at 923–1273 K (see Fig. 5). The comparative graph in Fig. 9 documents a much higher hot-formability of the CuCr0.6 alloy in com-

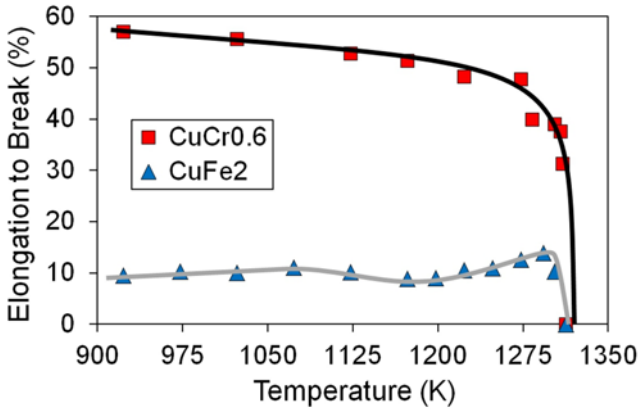

Fig. 9. Comparison of the hot-ductility of two selected copper alloys.

parison to the results of the CuFe2 alloy which have been previously achieved by the identical methodology [14]. The NDT values, however, are in the case of both materials almost identical.

3.3. Flow curves

The true stress-true strain curves were determined by 12 uniaxial compression tests. Parameters of heating of the samples Ø 8 mm × 12 mm were similar to the tensile tests. Tantalum foils were used to reduce the friction on the flat planes of the samples in contact with anvils. Forming temperatures of 923–1223 K and strain rates of 0.1–10 s^{-1} were applied, up to a true (logarithmic) height strain of 1.0. By the Origin software smoothed flow curves are presented in Fig. 10.

For all experimentally determined curves, both coordinates of the peak point were located, i.e. strain e_p (–) and maximum (peak) stress σ_p (MPa). Data for KFC copper were obtained by the digitization of the published flow curves. The measured σ_p-values were compared with those for KFC copper [20] and CuFe2 alloy [14]. In the comparative graph in Fig. 11, the CuCr0.6 alloy demonstrates the much higher flow stress values (approx. 50–80 % more than for KFC copper).

3.4. The hot deformation activation energy

Values of σ_p were used to calculate the hot deformation activation energy Q (kJ mol^{-1}) as described in details, e.g. in [21] and successfully applied to various alloys (see, e.g. [22, 23]). The hyperbolic law in the Arrhenius type equation is conventionally used for the description of the relation between quantities σ_p, T (K) and $\dot{e}$ (s^{-1}) [24]:

$$\dot{e} = C\exp\left(\frac{-Q}{RT}\right)\left[\sinh\left(\alpha\sigma_p\right)\right]^n, \qquad (1)$$

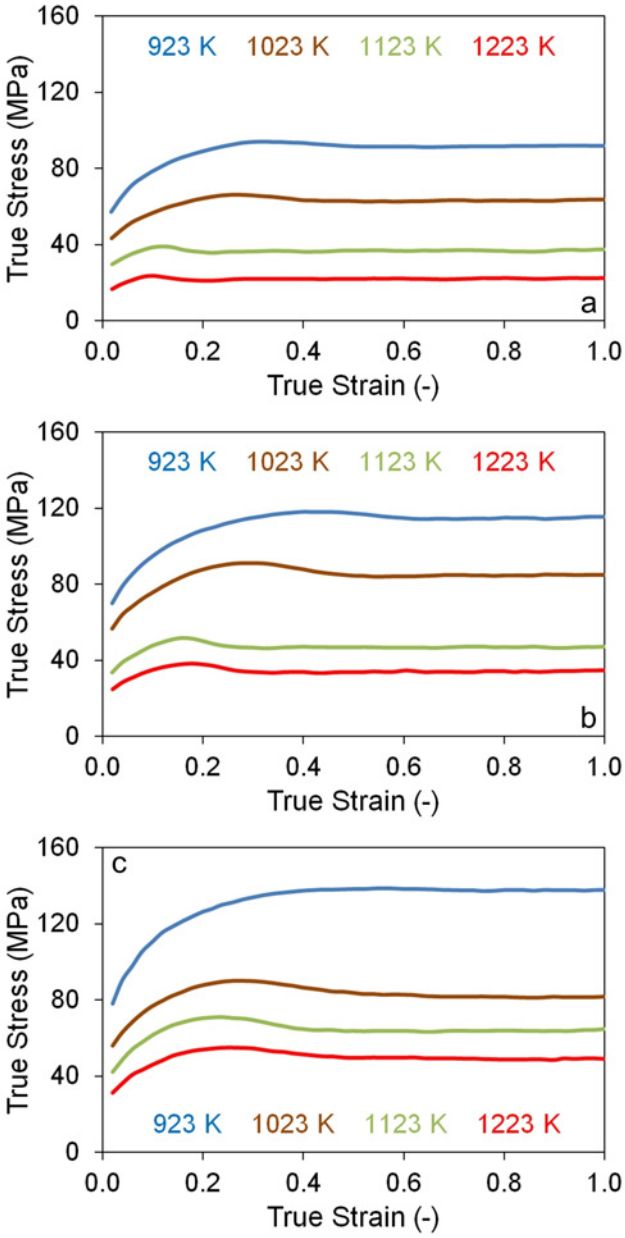

Fig. 10. Flow curves of the examined CuCr0.6 alloy in dependence on the temperature and strain rate: (a) strain rate of 0.1 s^{-1}; (b) strain rate of 1 s^{-1}; (c) strain rate of 10 s^{-1}.

where, besides the Q-value, quantities C (s^{-1}), n (–), and α (MPa^{-1}) are material constants.

Efficiency and accuracy of that constants' calculation were improved by the application of the specially developed interactive software ENERGY 4.0 [25]. The software uses the values of n and α, determined by simple regression analyses, only as of the first estimate of the parameters for the final refining nonlinear regression of all data corresponding to Eq. (1). Such a procedure ensures higher precision and reliability of results (i.e., a set of calculated constants Q, C, n, and α).

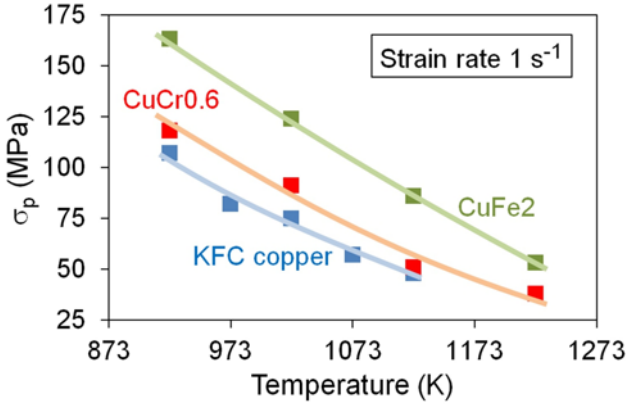

Fig. 11. Comparison of the σ_p-values of KFC copper, CuFe2 alloy, and CuCr0.2 alloy at various temperatures and selected strain rate level.

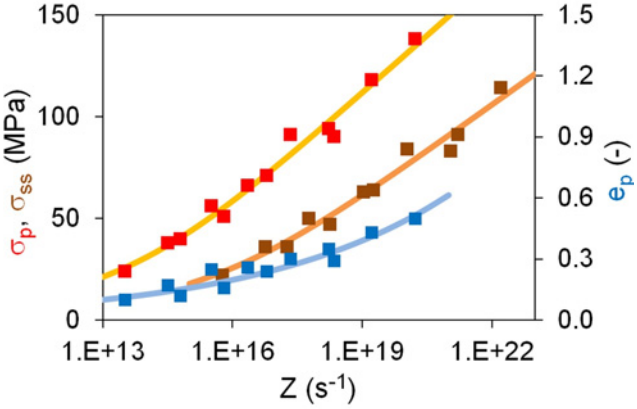

Fig. 12. Peak stress, steady-state stress, and peak strain for CuCr0.6 alloy in dependence on the Zener-Hollomon parameter.

This procedure yielded in the value of $Q = 340\,\mathrm{kJ\,mol^{-1}}$ for CuCr0.6 alloy, which allowed to calculate the values of Zener-Hollomon parameter $Z(\dot{e}, T)\,(\mathrm{s^{-1}})$. Subsequently, both coordinates of the peak point could be mathematically described, depending on the so-called temperature-compensated strain rate Z [26–28]:

$$Z = \dot{e} \exp\left(\frac{Q}{RT}\right), \tag{2}$$

where $R = 8.314\,\mathrm{J\,mol^{-1}\,K^{-1}}$ is the universal gas constant.

$$\sigma_p = \frac{1}{0.022} \operatorname{arcsinh} \sqrt[5.6]{\frac{Z}{5.96 \times 10^{14}}}, \tag{3}$$

$$e_p = 0.0054\, Z^{0.10}. \tag{4}$$

Analogically, the value of the hot deformation activation energy for the steady-state values σ_{ss} has been calculated. The value of $Q_{ss} = 393\,\mathrm{kJ\,mol^{-1}}$ is about 16 % higher than the value which was calculated from the peak-stress values. The following equation has been derived to describe the $\sigma_{ss}(Z)$-relation:

$$\sigma_{ss} = \frac{1}{0.026} \operatorname{arcsinh} \sqrt[5.8]{\frac{Z}{6.446 \times 10^{16}}}. \tag{5}$$

As documented in Fig. 12, the accuracy of the description of experimental data by Eqs. (3)–(5) is good over the entire range of deformation conditions.

Using the same methodology and applying the final non-linear regression in ENERGY software on the σ_p values, the activation energy of $284\,\mathrm{kJ\,mol^{-1}}$ was obtained for the KFC copper which is very close to the value of $289\,\mathrm{kJ\,mol^{-1}}$ calculated by Zhang et al. [20]. Moreover, the hot deformation activation energy of $380\,\mathrm{kJ\,mol^{-1}}$ was calculated for the CuFe2 alloy [14]. Zhang, Z. et al. [29] calculated the activation energy of $316\,\mathrm{kJ\,mol^{-1}}$ for the C194 copper alloy with iron and zinc additions. Zhang, Y. et al. [30] calculated the activation energy of $316\,\mathrm{kJ\,mol^{-1}}$ for the Cu-2Ni-0.5Si-0.15Ag alloy and the activation energy of $336\,\mathrm{kJ\,mol^{-1}}$ for the Cu-Cr-Zr alloy [31]. Gao et al. [13] studied the hot deformation behavior of a copper with different purities. The samples were compressed at the temperatures of 523–773 K under the strain rates of 10^{-4}–$10^{-1}\,\mathrm{s^{-1}}$. The Q-values were affected by materials purity, i.e., about $210\,\mathrm{kJ\,mol^{-1}}$ for the purities of 6 or 7 N, and $245\,\mathrm{kJ\,mol^{-1}}$ for the purity of 4 N of copper. According to [32], the hot deformation activation energy of $389\,\mathrm{kJ\,mol^{-1}}$ was calculated in the temperature range of 973–1173 K for the copper alloy with 3.45 % of Ti. Table 1 summarizes all the Q-values calculated for various copper-based materials. The higher Q-values of the Cu-Fe-P alloys may be associated with the Fe atoms, which can play a role of obstacles for the dislocations moving [29].

5. Conclusions

– The nil strength temperature of 1349 K and the nil ductility temperature of 1313 K were determined for the CuCr0.6 alloy, which are the unique results.

– In the temperature range from 923 K to approx. 1273 K, the formability of the examined alloy is very good and surprisingly monotonously growing with decreasing of forming temperature. This atypical deformation behavior is most obvious, especially in comparison with the previously tested CuFe2 alloy.

– The flow curves were obtained in the forming-temperature interval of 923–1223 K and the strain rate range of 0.1–$10\,\mathrm{s^{-1}}$. After their analysis, the val-

Table 1. The hot deformation activation energy of copper and Cu-based alloys

Material	Q (kJ mol^{-1}) for peak stress	Q (kJ mol^{-1}) for steady-state	Data source
Copper 6N	210		[13]
Copper 4N	245		[13]
KFC copper (0.13 % Fe)	284 (289)		[20]
C194 (2.34 % Fe, 0.13 % Zn)	316		[29]
Cu-2Ni-0.5Si-0.15Ag	316		[30]
Cu-Cr-Zr-Y	336		[31]
CuCr0.6	340	393	
CuFe2	380		[14]
Cu-3.45%Ti	389		[32]

ues of the hot deformation activation energy Q = 340 and 393 kJ mol^{-1} have been achieved from the peak-stress and steady-state-stress values, respectively. This proves that the value of the activation energy is influenced by the magnitude of the applied deformation.

– These activation energy values have been compared with the values which correspond to the forming of several Cu-based materials with the Q-values ranging from 210 to 389 kJ mol^{-1}.

– Throughout the deformation conditions, both coordinates of the peak point, as well as the steady-state stress, could be mathematically described with good accuracy by relationships depending on the Zener-Hollomon parameter.

– Calculated peak strain value corresponds to the start of dynamic recrystallization, which is relatively easy to initiate in the investigated alloy. Peak stress is the value appropriate for a simple and fast prediction of the maximum flow stress in dependence on the temperature-compensated strain rate.

Acknowledgements

The paper was created thanks to the project No. CZ.02.1.01/0.0/0.0/17_049/0008399 from the EU and CR financial funds provided by the Operational Programme Research, Development and Education, Call 02_17_049 Long-Term Intersectoral Cooperation for ITI (Managing Authority: Czech Republic – Ministry of Education, Youth and Sports), as well as the student grant projects SP2019/86 and SP2019/43 (VŠB-TU Ostrava).

References

[1] Dobatkin, S. V., Gubicza, J., Shangina, D. V., Bochvar, N. R., Tabachkova, N. R.: Materials Letters, *153*, 2015, p. 5. doi:10.1016/j.matlet.2015.03.144

[2] Rodak, K: Microstructure and Properties. London, IntechOpen 2017. doi:10.5772/intechopen.68954

[3] https://southerncopper.com/nonferrous-metals/c18200-chromium/

[4] Vinogradov, A., Patlan, V., Suzuki, Y., Kitagawa, K., Kopylov, V. I.: Acta Mater., *50*, 2002, p.1639. doi:10.1016/S1359-6454(01)00437-2

[5] Xu, C. Z., Wang, Q. J., Zheng, M. S., Zhu, J. W., Li, J. D., Huang, M. Q., Jia, Q. M., Du, Z. Z.: Mater. Sci. Eng. A, *459*, 2007, p. 303. doi:10.1016/j.msea.2007.01.105

[6] Wei, K. X., Wei, W., Wang, F., Du, Q. B., Alexandrov, I. V., Hu, J.: Materials Science and Engineering A, *528*, 2011, p. 1478. doi:10.1016/j.msea.2010.10.059

[7] Islamgaliev, R. K., Nesterov, K. M., Bourgon, J., Champion, Y., Valiev, R. Z.: Journal of Applied Physics, *115*, 2014, p. 194301. doi:10.1063/1.4874655

[8] Rodak, K., Brzezińska, A., Molak, R.: Materials Science & Engineering A, *724*, 2018, p. 112. doi:10.1016/j.msea.2018.03.077

[9] Stobrawa, J., Rdzawski, Z., Głuchowski, W., Malec, W.: Archives of Metallurgy and Materials, *56*, 2011, p. 171. doi:10.2478/v10172-011-0020-1

[10] Jung, T., Kwaśny, W., Rdzawski, Z., Głuchowski, W., Matus, K., Pawlyta, M., Szindler, M.: Archives of Metallurgy and Materials, *62*, 2017, p. 2441. doi:10.1515/amm-2017-0359

[11] Rdzawski, Z., Stobrawa, J., Głuchowski, W., Sobota, J.: Archives of Metallurgy and Materials, *59*, 2014, p. 649. doi:10.2478/amm-2014-0106

[12] Rodak, K., Urbańczyk-Gucwa, A., Jabłońska, M. B.: Archives of Civil and Mechanical Engineering, *18*, 2018, p. 500. doi:10.1016/j.acme.2017.07.001

[13] Gao, W., Belyakov, A., Miura, H., Sakai, T.: Mater. Sci. Eng. A, *265*, 1999, p. 233. doi:10.1016/S0921-5093(99)00004-0

[14] Schindler, I., Sauer, M., Kawulok, P., Rodak, K., Hadasik, E., Jabłońska, M. B., Rusz, S., Ševčák, V.: Archives of Metallurgy and Materials, *64*, 2019, p. 701. doi:10.24425/amm.2019.127601

[15] Chakrabarti, D. J., Laughlin, D. E.: Bulletin of Alloy Phase Diagrams, *5*, 1984, p. 59. doi:10.1007/BF02868727

[16] Kotásek, O., Rusz, S., Schindler, I., Kawulok, P., Opěla, P.: In: Proceedings of the 27th International Conference on Metallurgy and Materials 2018. Ostrava, Tanger Ltd. 2018, p. 401. ISBN: 978-808729484--0.

[17] Kawulok, P., Schindler, I., Kawulok, R., Rusz, S., Opěla, P., Kliber, J., Kawuloková, M., Solowski,

Z., Čmiel, K. M.: Metalurgija, *55*, 2016, p. 365. http://hrcak.srce.hr/file/226320
[18] Turchanin, M. A.: Powder Metallurgy and Metal Ceramics, *45*, 2006, p. 457. doi:10.1007/s11106-006-0106-x
[19] https://southerncopper.com/www/cabinet/scscat182cl2.pdf
[20] Zhang, H., Zhang, H. G., Peng, D. S.: Metal Soc., *16*, 2006, p. 562. doi:10.1016/S1003-6326(06)60098-8
[21] Schindler, I., Bořuta, J.: Arch. Metall., *39*, 1994, p. 479.
[22] Legerski, M., Plura, J., Schindler, I., Rusz, S., Kawulok, P., Kulveitova, H., Hadasik, E., Kuc, D., Niewielski, G.: High Temper. Mater. Process., *30*, 2011, p. 63. doi:10.1515/htmp.2011.008
[23] Schindler, I., Kawulok, R., Kulveitová, H., Kratochvíl, P., Šíma, V., Knapiński, M.: Acta. Phys. Pol. A, *122*, 2012, p. 610. https://www.researchgate.net/publication/286970815
[24] Sellars, M. C., Tegart, W. J. McG.: Int. Metall. Rev., *17*, 1972, p. 1. doi:10.1179/imtlr.1972.17.1.1
[25] Schindler, I., Kawulok, P., Kawulok, R., Hadasik, E., Kuc, D.: High Temp. Mater. Proc., *32*, 2013, p. 149. doi:10.1515/htmp-2012-0106
[26] Zener, C., Hollomon, J. H.: J. Appl. Phys., *15*, 1944, p. 22. doi:10.1063/1.1707363
[27] Kliber, J., Schindler, I., Kubinski, W., Kuzminski, Z.: Steel Res., *60*, 1989, p. 503. doi:10.1002/srin.198901693
[28] Momeni, A., Dehghani, K.: Met. Mater. Int., *16*, 2010, p. 843. doi:10.1007/s12540-010-1024-5
[29] Zhang, H., Zhang, H. G., Li, L. X.: J. Mater. Process. Technol., *209*, 2009, p. 2892. doi:10.1016/j.jmatprotec.2008.06.048
[30] Zhang, Y., Volinsky, A. A., Xu, Q. Q., Chai, Z., Tian, B., Liu, P., Tran, H. T.: Metall and Mat Trans A, *46*, 2015, p. 5871. doi:10.1007/s11661-015-3150-7
[32] Zhang, Y., Chai, Z., Volinsky, A. A., Tian, B., Sun, H., Liu, P., Liu, Y.: Mater. Sci. Eng. A, *662*, 2016, p. 320. doi:10.1016/j.msea.2016.03.033
[32] Hameda, A., Blaz, L.: Mater. Sci. Eng. A, *254*, 1998, p. 83. doi:10.1016/S0921-5093(98)00753-9